Bioactive Materials 5 (2020) 458–467

Contents lists available at ScienceDirect

Bioactive Materials

journal homepage: http://www.keaipublishing.com/biomat

Additive manufacturing of biodegradable porous orthopaedic screw

Ramya Dhandapani[c], Priya Dharshini Krishnan[c], Allen Zennifer[c], Vishal Kannan[c], Amrutha Manigandan[c], Michael R. Arul[a], Devina Jaiswal[b,a], Anuradha Subramanian[c], Sangamesh Gurappa Kumbar[a,**], Swaminathan Sethuraman[c,*]

[a] Department of Orthopaedics, UConn Health, Farmington, CT, 06030, USA
[b] Department of Biomedical Engineering, Western New England University, Springfield, MA, 01119, USA
[c] Centre for Nanotechnology & Advanced Biomaterials, SASTRA Deemed University, Thanjavur, 613401, India

ARTICLE INFO

Keywords:
3D printing
Orthopaedic screws
Biodegradable
Porous screws

ABSTRACT

Advent of additive manufacturing in biomedical field has nurtured fabrication of complex, customizable and reproducible orthopaedic implants. Layer-by-layer deposition of biodegradable polymer employed in development of porous orthopaedic screws promises gradual dissolution and complete metabolic resorption thereby overcoming the limitations of conventional metallic screws. In the present study, screws with different pore sizes (916 × 918 μm to 254 × 146 μm) were 3D printed at 200 μm layer height by varying printing parameters such as print speed, fill density and travel speed to augment the bone ingrowth. Micro-CT analysis and scanning electron micrographs of screws with 45% fill density confirmed porous interconnections (40.1%) and optimal pore size (259 × 207 × 200 μm) without compromising the mechanical strength (24.58 ± 1.36 MPa). Due to the open pore structure, the 3D printed screws showed increased weight gain due to the deposition of calcium when incubated in simulated body fluid. Osteoblast-like cells attached on screw and infiltrated into the pores over 14 days of *in vitro* culture. Further, the screws also supported greater human mesenchymal stem cell adhesion, proliferation and mineralized matrix synthesis over a period of 21 days *in vitro* culture as compared to non-porous screws. These porous screws showed significantly increased vascularization in a rat subcutaneous implantation as compared to control screws. Porous screws produced by additive manufacturing may promote better osteointegration due to enhanced mineralization and vascularization.

1. Introduction

Every year osteoporosis affects 8.9 million individuals globally resulting in an osteoporotic fracture for every 3 s [1]. Fracture may also be accompanied with several pathological conditions such as cancers, osteogenesis imperfecta [2]. Rigid internal fixation devices, mainly orthopaedic screw, escalates healing and mobility of injured tissues by reducing fracture gap and provide compression across the fractured bones [3]. Optimal healing of bone fractures mainly depends on complete immobilization, preservation of bone segments, bone ingrowth with the reestablishment of local blood vessels [4]. However, gold standard orthopaedic screws made of titanium or stainless steel are excessively stiff causing wear and tear in the neighboring tissues [5]. Higher elastic modulus of metallic screws relative to normal bone leads to “stress shielding” effect that results in localized osteopenia [6]. Further, robust integration between screw thread and neighboring bony tissue complicates the revision surgery during the removal of screws [7]. This has led to the use of biodegradable screws made of polymers such as poly(lactic-co-glycolic acid) (PLGA), poly(L-lactic acid) (PLLA), which avoids the need for secondary surgery [8–11]. Department of Orthopaedics and Traumatology at Central Hospital in Finland treated seven patients with malleolar fractures and syndesmotic separations with self-reinforced poly(glycolic acid) (SR-PGA) screws to repair the syndesmosis and results showed that all patients yielded an acceptable response with a stable ankle mortise [12]. PLLA screws comprising hydroxyapatite and β-tricalcium phosphate such as BioRCL, Biosteon,

Peer review under responsibility of KeAi Communications Co., Ltd.
* Corresponding author.
** Corresponding author. Department of Orthopaedic Surgery, Department of Biomedical Engineering, Department of Materials Science and Engineering, The University of Connecticut, Farmington, CT, 06030-1320, USA.
E-mail addresses: ramya.d2003@gmail.com (R. Dhandapani), p.dharshi14@gmail.com (P.D. Krishnan), allenzennifer2@gmail.com (A. Zennifer), vishkann22@gmail.com (V. Kannan), amru1812@gmail.com (A. Manigandan), arul@uchc.edu (M.R. Arul), devina.jaiswal@wne.edu (D. Jaiswal), anuradha@bioengg.sastra.edu (A. Subramanian), kumbar@uchc.edu (S.G. Kumbar), swami@sastra.edu (S. Sethuraman).

https://doi.org/10.1016/j.bioactmat.2020.03.009
Received 24 October 2019; Received in revised form 11 March 2020; Accepted 18 March 2020

Biocryl etc., are commercially available for clinical applications. However, long term study with patients implanted with biodegradable PLLA screws showed tunnel widening, sterile abscess formation and intra-articular migration [13]. Hydrolytic degradation of PLGA or PLLA release acidic by products that inhibit angiogenesis and decrease the bone cell recruitment at site of implantation thereby causing foreign body reactions and fluid effusion [14].

Magnesium based interference screws possessing comparable elastic modulus with native bone showed better mineralization at inter-zone and thereby enhanced the tendon-bone junction healing [8,15]. However, the rapid corrosion rate of magnesium alloys and its toxic by-products made it unfit to be used as fixation device [10]. Polyglycolic acid (PGA) screws showed improved bone-remodeling by gradual stress transfer to bone but initiation of sterile sinus formation lead to improper dynamics between device strength retention and wound healing [12]. These lacunas were overcome by machine cut silk screws and plates that possessed excellent mechanical strength and biocompatibility (FDA approved biomaterial) [11]. Although the desirable mechanical strength was achieved with existing biodegradable screws, complete healing remains challenging as the fracture healing requires the re-establishment of blood vessel network and osseous ingrowth. Scaffolds for bone tissue regeneration have been developed with controlled porosity to enhance cell infiltration and supply of nutrients that stimulated the bone remodeling and repair [16,17]. Presence of interconnected pores in bone scaffolds have shown enhanced vascularization of the ingrown tissue and infiltration of cells to grow into desired physical form minimizing the recovery time [18–20]. Average pore size of 250–300 μm supported cellular infiltration and capillary formation thereby promoting osseous growth whereas pores < 100 μm favor hypoxic induced cartilage formation [21]. However, current screw manufacturing techniques such as machining of metallic screws and injection moulding of polymeric resorbable screws fail to establish the interconnected porous structures throughout the biodegradable screws [22].

Integration of additive manufacturing technology in orthopaedic healing has emanated highly precise and large scale manufacturing of patient–specific prosthetics and implants through 3D scanning, 3D reconstruction and digital processing of patient data [23]. Complex mesh structures with improved design and functionality are achievable using metal powder bed fusion method (laser and electron beam powered) or fused deposition modeling, thereby reducing the manufacturing costs and lead-times compared to the conventional techniques [24,25]. Thus additive manufacturing of porous orthopaedic implants would promote the custom-manufacturing of implants for trauma patients [26]. Recently, 3D printed Gemcitabine/Methotrexate-loaded PLA screws (4 mm) showed infill pattern and density dependent mechanical strength and anti-bacterial properties with enhanced cytotoxicity towards osteosarcoma cells [27]. However, there are no reports on *in vivo* biocompatibility and efficacy of pore size and porosity on mineralization & vascularization potential of the orthopedic screws which is ultimatum for bone regeneration. In the present study, cortical screws with tunable porosity were developed using additive manufacturing technology (AMT), which facilitates the fabrication of complex structures with high accuracy, low cost, rapid product development and design freedom [28,29]. Poly(lactic acid) (PLA) cortical screws with porous interconnections were developed by fused deposition modeling by optimizing the various printing parameters such as layer height, fill density travel speed and printing speed. These screws were characterized for both compressive and torsional strengths to determine their suitability for fixation during fractures. The role of porous interconnections in the biodegradable screws on establishing mineralized matrix *in vitro* were examined by culturing osteoblast-like cells (MG-63 cell line) and human mesenchymal stem cells. The preliminary *in vivo* subcutaneous implantation studies were performed to evaluate the local inflammatory response around the implanted region and role of interconnected pores in vascularization.

2. Materials and methods

2.1. Materials

PLA filament (1.75 mm filament diameter) purchased from Reddx Technologies Pvt Ltd, Sodium chloride, Sodium Bicarbonate, Tris (Hydroxy-methyl) amino methane, Magnesium Chloride hexa-hydrate, Sodium Sulfate were purchased from Merck Life Science, India. Potassium phosphate dibasic tri-hydrate was purchased from Himedia, India. Potassium chloride and Calcium chloride were purchased from Qualigens and Chemspure, India respectively. MTT (Sigma, India), MTS assay kit (Promega), Invitrogen Quant-iT PicoGreen dsDNA assay kit (Eugene, Oregon, USA), Live dead assay kit (Molecular probes, Thermo Fisher), Alizarin red, Dulbecco's Modified Eagle Medium (DMEM-HG) (Lonza, USA) were procured.

2.2. Methods

2.2.1. Fabrication of porous screw

Cortical screws were designed using AUTOCAD Software with dimensions matching the commercially available titanium screws (4.5 mm, GPC Medical Ltd., WHO-GMP surgical instruments, Malaysia). The designs obtained in STL format were fed to CURA software to convert file into machine readable GCODE. The designed screw was printed using PLA filament in 3D printer (HYDRA 200) by maintaining printing and bed temperature at 210 °C and 70 °C, respectively. Fill density (FD), one of the printing parameter was varied to understand its effect on pore size and total porosity of the developed screws. Printing parameters such as print speed, travel speed and layer height were varied to achieve screws with desired specifications without any disfigurement.

2.2.2. Scanning electron microscopy

The morphology of the pores, pore dimensions with the thickness of printed motifs was analyzed using SEM (Vega 3, TESCAN) at an accelerating voltage of 5 kV. The sample placed on stub was sputter coated with thin film of gold using an auto sputter fine coater (JFC 1600, JEOL, Japan) prior to imaging. For each of these measurements we used a sample size of n = 3 for each type and a minimum of 100 pores were used and reported as mean ± SD.

2.2.3. Micro CT analysis

The cortical screws were scanned using Skyscan 1176 Micro CT Imaging System without filter to evaluate open porosity, closed porosity and total porosity values. Reconstruction of datasets was performed in NRecon software by adjusting ring artifacts and misalignment. CTan software was used to estimate the porosity values without altering threshold values between samples. Porosity was calculated by the software based on the following formula where open and closed pores define interconnectivity and voids surrounded by solid in the screw, respectively.

$$Closed\ \ Porosity = \frac{Volume\ \ of\ \ closed\ \ pores}{Total\ \ volume\ \ of\ \ VOI} \times 100$$

$$Open\ \ Porosity = \frac{Volume\ \ of\ \ open\ \ pores}{Total\ \ volume\ \ of\ \ VOI} \times 100$$

For each of these measurements we used a sample size of n = 3 for each type and results were reported as mean ± SD.

2.2.4. Mechanical properties

The compressive strength of porous screws was evaluated using INSTRON mechanical tester at a preload of 10 kN and at the displacement rate of 1 mm/s while keeping solid screws as control. The maximum load, compressive strength and elastic modulus of the screws were calculated from the stress versus strain curve. Automated torsional

assay was performed for screws of different fill densities (45% and 100%) at n = 6 screws/group in Instron apparatus. The measurements were performed according to standard (ASTM F2502) with the screws of 22.5 mm long with 3.8 mm diameter. The head portion of the screw was fixed at the rotatory drill chuck of torque cell with the other end fixed to the static portion. The screws were tested for torsional properties at 1 revolution/min in clockwise polarity. Torque versus rotation graph was recorded to study the torsional properties of polymeric screws. For these studies, dry samples of minimum six per group were used and the results were presented as mean ± standard error.

2.2.5. In vitro degradation profile

In vitro degradation rate of screws were evaluated by immersing in simulated body fluid (SBF), which has ion concentrations identical to human plasma [30]. The degradation profile of screws of known initial weights (45%- 0.352 ± 0.002, 100%- 0.455 ± 0.004) were followed up to five months in SBF at pH 7.4 maintained at 37 °C. SBF Solution (5 ml) was replaced every alternate day with fresh medium to prevent saturation of the fluid. The samples were collected at predetermined time points and measured for weight loss and stained with alizarin red (40 mM) followed by subsequent washing using DI water to observe salt deposition. For each of these measurements, we used a sample size of n = 6 for each type screw and each time point. The results were reported as mean ± standard error.

$$Degradation\ \ Rate = \frac{Initial\ \ weight - Final\ \ Weight}{Initial\ \ weight} \times 100$$

3. Osteogenic evaluation

3.1. Cell lines and culture conditions

Human bone marrow derived mesenchymal stem cells (BMSCs) were purchased from Millipore (Millipore Sigma, USA) and cultured in basal media comprising DMEM (High Glucose supplemented with 10% fetal bovine serum) and 1% penicillin–streptomycin as per supplier protocol. Osteogenic media composed of basal media with 0.2 mM L-ascorbic acid and 7.0 mM glycerol 2-phosphate disodium salt and 0.1 mM dexamethasone. MG63 cell line, osteoblast like cells, was maintained in DMEM medium supplemented with 10% FBS and 1% penicillin–streptomycin. Screws were soaked in basal media overnight and each screw was seeded (10,000 cells/well, passage 5) in 48 well plate with basal media and then switched to osteogenic media following 24 h. The media was changed every alternate day until predetermined time point and screws seeded without cells were used as control. All studies were done in triplicate for each time point and each group of scaffolds.

3.2. Metabolic activity

Metabolic activity was measured by culturing MG63 osteoblast cell line on porous screws, non-porous screws and TCPS at predetermined time intervals (1, 3, 7 and 14 days). Screws were sterilized by dipping in 70% ethanol and UV sterilized for 1 h prior seeding. Cells of density 6×10^3 cells/well (passage number 39) were seeded over the screws and media was changed every other day up to 14 days. TCPS was used as control and were done in triplicate for each time point and each group. MTS assay was performed as per the manufacturer's protocol and absorbance was measured at 490 nm using a microplate reader (Tecan Infinite M200, Austria). A sample size of n = 3 for each time point and results were presented as mean ± standard error.

3.3. Cell proliferation

The rate of hMSCs proliferation after transferring to osteogenic media was quantified by measuring the amount of cellular DNA content at various time points (day 7, 14 and 21) using a Picogreen dsDNA assay. In brief, the cellular constructs at different time points were washed twice with PBS, transferred to new well plates and 1 mL of 1% Triton X-100 solution was added to lyse the cells. The well plates underwent three freeze–thaw cycles, between −70 °C and room temperature, and mixed with the aid of a pipette to extract cell lysate from the screws prior to analysis. Fluorescence was measured at excitation of 485 nm and emission of 535 nm using BioTek plate reader and converted to DNA concentration (μg/ml) using a standard curve. A sample size of n = 3 for each time point and results were presented as mean ± standard deviation.

3.4. Live/dead assay

Screws were collected at predetermined time points (1, 5, 7, 14 days) and stained using live/dead assay kit as per manufacturer's protocols. Screws were imaged under confocal microscopy (FV1000, Olympus, Japan). Viability of BMSCs on the screws was imaged on post-osteoinduction using a fluorescence microscope (Nikon Instruments Inc, Melville, USA) at 10X magnifications to view the cells independently and along with the scaffolds.

3.5. Cell adhesion assay

Cell adhesion and expansion on screws were observed under SEM after sputter coating. Screws were fixed using 4% paraformaldehyde, dehydrated using increasing concentrations of ethanol and stored in vacuum desiccator until imaging under SEM (VEGA3, Tescan).

3.6. Alizarin red assay

Mineralized matrix deposition by osteoinduced BMSCs on solid and porous screws was evaluated as marker of mature osteoblast phenotype using alizarin red staining method for calcium deposition (7, 14, 21 days). Screws were stained with 40 mM alizarin red solution for 10 min at room temperature and washed with distilled water to remove unabsorbed dye and optical images were taken. A sample size of n = 6 for each time point and results were presented as mean ± standard deviation.

3.7. Alkaline phosphatase assay

The activity of phenotypic bone marker alkaline phosphatase was assessed based on the hydrolysis of p-nitrophenyl phosphate to p-nitrophenol. MG63 osteoblasts cell line were cultured in porous screws, non-porous screws and TCPS and assay was performed at predetermined time intervals of 1, 3, 7, 14 and 21 days using alkaline phosphatase kit as per manufacturer's protocol. In brief, the osteoblasts cultured porous screws, non-porous screws and TCPS were washed twice with DPBS and 200 μL of 1% triton-X was added to lyse the cells. Then 100 μL of cell lysate was added to 400 μL of the substrate and incubated for 30 min at 37 °C. The reaction was stopped by the addition of 0.4 M sodium hydroxide solution and absorbance was measured at 410 nm using multi-well plate reader (Tecan Infinite 200 M, USA). A sample size of n = 3 for each time point and results were presented as mean ± standard error.

3.8. In vivo biocompatibility

In vivo biocompatibility studies was performed by subcutaneous implantation of screws in male Wistar Rats (*Rattus Norvegicus*) for evaluating the inflammatory responses. Total 18 animals (200–250 g) were randomly divided into two groups (n = 9) for this study. All animals were housed in an individual cage in a temperature-controlled facility. The surgical procedures were approved by Institutional Animal Ethics Committee at SASTRA University (451/SASTRA/IAEC/RPP). 3D

printed screws were soaked in 70% ethanol overnight and UV irradiated for 1 h and stored in sterile container until implantation. Intraperitoneal injections of ketamine (50 mg/kg body weight) and xylazine (20 mg/kg body weight) were administrated to anesthetize the animals. The neck region of the animal was shaved and sterilized with 70% ethanol solution. Using a sterile surgical blade no. 22 (Gillette, India), an incision of about 12 mm was made on the dorsum of animals. A subcutaneous pouch was created on either sides of the incision and the implant was inserted into each pocket. Upon implantation of the screw, the incision was sutured using a non-absorbable surgical suture (Chromic, India). The animals were sacrificed at predetermined time points (4, 8, and 12 weeks) and tissues were collected for histopathological studies. At the end of each time point (4, 8, and 12 weeks), rats were euthanized using an overdose of pentobarbital (75 mg/kg) followed by carbon-dioxide asphyxiation. The implants and surrounding tissue were excised and fixed in 10% formalin solution for 7 days. Before embedding in paraffin wax, the tissue samples were dehydrated in an Automatic Tissue Processor (Leica TP1020, Leica Microsystems, Germany) by transferring through a series of gradually increasing percentages of alcohol. The tissue samples were embedded in paraffin using embedding machine (EG1150 H&C, Leica Microsystems, Germany), sectioned using a microtome (Rotary Microtome Leica RL2125RT, Leica Microsystems, Germany) and stained with hematoxylin and eosin. These samples were viewed under light microscope (Nikon, eclipse, C1-L, Japan) to determine the average number of different inflammatory cell types present in the tissue surrounding implant and the tissue reaction was rated as per ISO 10993-6.

3.9. Statistics

Sample sizes used for each characterization are identified above. All the results are presented in the form of mean ± SD/SE, with n equal to the number of samples analyzed. Student *t*-test was performed to determine the effects of fill density (FD) on scaffold compressive modulus and the ability to promote neovascularisation *in vivo*. One way analysis of variance (ANOVA) was performed to determine the influence of FD on in *vitro* degradation of the cortical screw. All analyses were performed using the SPSS statistical software package.

4. Results

4.1. Fabrication of porous screw stem

Ability to alter pore dimensions and pore size distribution using 3D printing technology was first investigated in cylindrical stem of different diameters. Screw stem of 5 × 10 mm were printed to match the dimensions of commercially available cortical screws (Fig. 1 a-d) by varying travel speed, print speed and layer height at constant FD (25%). At a constant layer height (0.1 mm) and print speed (10 mm/s), screw stems were printed by varying travel speeds (50 mm/s and 20 mm/s). The structural stability was lost during printing process, which may be attributed to the mismatch between print speed and travel speed (Fig. 1a and b). Hence the print speed was further reduced to 5 mm/s while keeping the other parameters as constant. However, the stem structure was distorted after certain layers (Fig. 1c) due to fusion of adjoining layers. Hence, the distance between individual layers were increased to 0.2 mm by adjusting layer height and screw stem with the specified dimension (5 × 10 mm) were printed without any disfigurement (Fig. 1d). Further FD was varied as 25, 45, 55, and 65% to alter the pore dimensions in screw stem while keeping the print speed, travel speed and layer height at 5 mm/s, 20 mm/s and 0.2 mm, respectively, as constant. Fig. 1 e-h shows that the number of pores increase with increase in FD and eventually, leading to decrease in pore size in 5 mm cylinders.

Fig. 1(i–p) shows the scanning electron micrographs of porous screw stem with varying FD. Increase in FD changed the pore size (Fig. 1 i-l) and thickness (Fig. 1 m-p) of motif as observed through SEM (Table 1). Pore size and thickness of layers were observed to be reduced at higher FD. Also, the number of strands was increased at increasing FD, which in turn directly reduces the distance between the strands and subsequent increase in the aspect ratio of the pores.

4.2. 3D printing of porous cortical screw

Screws with the specific dimensions (Table 2) equivalent to commercially available metallic cortical screws were designed using AUTOCAD (Fig. 2a). The screw CAD design had been converted into.stl file (Fig. 2b) and the same was printed using FDM technique (Fig. 2c). Micro CT images of 3D printed screw (Fig. 2d) confirmed the structural similarity of commercially available 4.5 mm cortical screw with 1.5 mm pitch size. SEM images showed the layer-by-layer deposition of PLA filament forming a rough tapered end for easy fixation of screws (Fig. 2 e-g).

4.3. Porosity analysis of the screw

Porosity including open and closed porosity of the printed cortical screws with varying FD measured using μCT were imaged and graphically represented (Fig. 3 a-d). Sagittal sections of screws show the distribution of pores throughout screw surface for varying fill densities. Screws exhibited comparable open porosity at 25% and 45% FD whereas significant reduction of open porosity were obtained in screws with 65% FD ($p < 0.05$). For further characterization, porous screws with 45% FD were chosen as the pore size of 259 × 207 μm is desirable for bone ingrowth [31–33].

4.4. In vitro degradation profile

The degradation rate of porous and solid screws was determined in simulated body fluid (SBF) as it mimics ion concentration with human blood plasma by measuring the weight loss percentage (Fig. 3e). The percentage weight of porous screws was observed to increase at 1 week up to 6 weeks whereas solid screws exhibited weight gain at 2–4 weeks. Weight loss was evident only after 8 weeks for both porous and solid screws though the screw structure was intact. Further alizarin red staining of the screws confirmed the presence of calcium salt deposition majorly in the head region of screws (Fig. 3f).

4.5. Mechanical properties

The compression test performed on porous and solid screws (Table 3) showed no significant difference between the maximum compressive strength. Elastic modulus estimated from stress versus strain curve showed no significant difference. Torsional properties for screws measured a peak torque of 0.38 ± 0.038 Nm and 0.53 ± 0.017 Nm respectively for solid (100%) and porous (45%) screws.

4.6. MG 63 cell proliferation and functionality assessment

Fig. 4a and b shows the scanning electron micrographs of MG63 cells adhering on the surface of porous screws after three days of culture. Number of viable cells in porous screws increased significantly up to 14 days (Fig. 4c) than non-porous screws and TCPS ($p < 0.05$). Live-dead assay confirmed the occurrence of viable cells inside the porous structures and homogenous distribution of viable cells were noticed all over the porous structures at all time points (till 14 days) (Fig. 4 d-g). ALP activity of cells cultured on porous and solid screws was determined from day 1 to day 14 compared to control group (Fig. 4h). Significantly higher ALP activity in porous screws than solid screws and TCPS control ($p < 0.05$) confirmed the role of porosity in maintaining the osteoblast phenotype and matrix maturation.

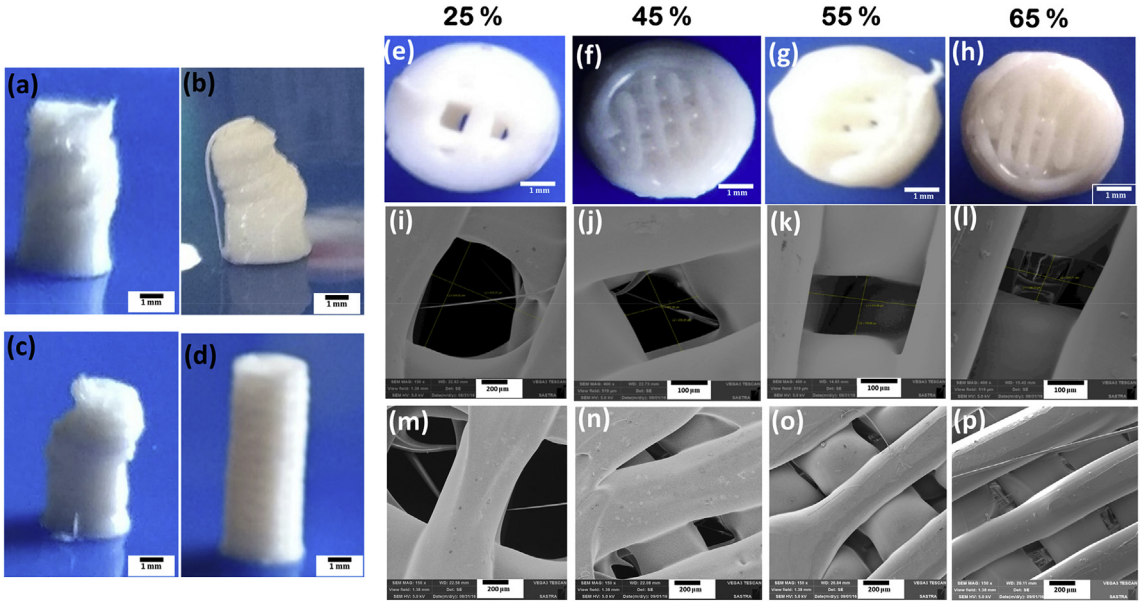

Fig. 1. Optical Images of 5 mm diameter printed cylinders with 0.1 mm layer height while varying printing & travel speeds (PS, TS) (a) 10, 50 mm/s; (b) 10, 20 mm/s (c) 5, 20 mm/s; (d) while undistorted structure was obtained at 5, 20 mm/s & 0.2 mm layer height; (e–h) FD were varied at 25%, 45%, 55%, & 65%, respectively and (i–l) shows decreasing pore dimensions (scale bar- 100 μm) & (m–p) reduced thickness of strands from SEM Analysis (scale bar- 200 μm).

Table 1
Porosity evaluation using SEM (sample size of n = 3 and a minimum of 100 pores were used).

Fill Density (%)	Pore Dimension (width × length) (μm)	Layer thickness (μm)
25	916 x 918	500 ± 90
45	259 x 207	590 ± 23
55	311 x 180	350 ± 25
65	254 x 146	300 ± 56

Table 2
Dimensions for designing and printing parameters for 3D printing of screws.

Specifications of designed cortical screw	
Head diameter	8.0 mm
Core diameter	3.5 mm
Thread diameter	5.0 mm
Pitch	1.5 mm
Hexagonal socket width	3.2 mm
Socket depth	3.0 mm
Screw height	20 mm

4.7. Osteogenic differentiation of BMSCs

DNA quantification was performed for *BMSCs* cultured porous and solid screws to determine the cell number at various time points (Fig. 5a). There was no significant difference between porous and solid screws until day 14 however porous screws showed significant reduction in cell number. Alizarin red S staining was carried out for both the screws cultured BMSCs on day 7 and 14 to determine the calcium deposits (Fig. 5b). Screws printed at FD 45% cultured with BMSCs exhibited positive staining of Alizarin red at 7 and 21 days where the red color became prominent at day 21 indicating mineralization and osteoblast differentiation of the BMSCs on the porous screws. However, no color change was observed in solid screws up to 21 days though the cell number appeared to be comparable on both the screws. Further, live-dead assay demonstrates the distribution of viable cells on both the screws (Fig. 5c).

4.8. In vivo biocompatibility

Fig. 6 a-g shows the creation of a sterile pouch and implantation of the printed screws in the subcutaneous region of the rats. All animals were healthy and no behavioral changes were observed during the study. The sutures used for wound closure degraded within 1 week and there was no significant weight loss in animals. Implanted screws did not cause any local irritation and was categorized as non-irritant material as per the ISO 10993-6-2001. Histology evaluation showed presence of lymphocytes and negligible giant cells around the implant showing a mild inflammatory response after 4 weeks (Fig. 7). However, inflammation was not evident by the end of 12 weeks in both the groups. Abscess formation, tissue necrosis and acute inflammation were absent in both the groups. Minimal amount of fat associated with the fibrosis was observed in the implant site of the porous screws whereas the group of fat cells was observed to be elongated in the implanted region of solid screws. The extent of neovascularisation were significantly noted as broad capillaries associated with fibroblastic structures within 1 week and increased up to 12 weeks in porous screws (45% FD) compared to solid screws (100% FD).

5. Discussions

Evolution of metallic orthopaedic implants could not overcome the major pitfalls manifesting restricted tissue ingrowth, metal ion accumulation, implant migration, and related complications in healing leading to removal of permanent orthopaedic devices [34]. Fabrication of biodegradable screws with desirable mechanical strength facilitate the osseous ingrowth by controlled degradation of biomaterials. Since rapid fracture healing mainly depends on angiogenesis process, introducing interconnectivity throughout the orthopaedic screws would fasten clinical reunion of the fractured bone ends. With additive manufacturing technique, pores of uniform size can be introduced all over the implantable screws by computer-aided designing. In this study, biodegradable cortical screws have been customized with porous interconnections by CAD modelling and FDM technique. Additive manufacturing technology offers rapid fabrication of screws at large scale with high reproducibility, precision and controllable porous interconnections [35]. Screw stem (5 × 10 mm) had been printed without

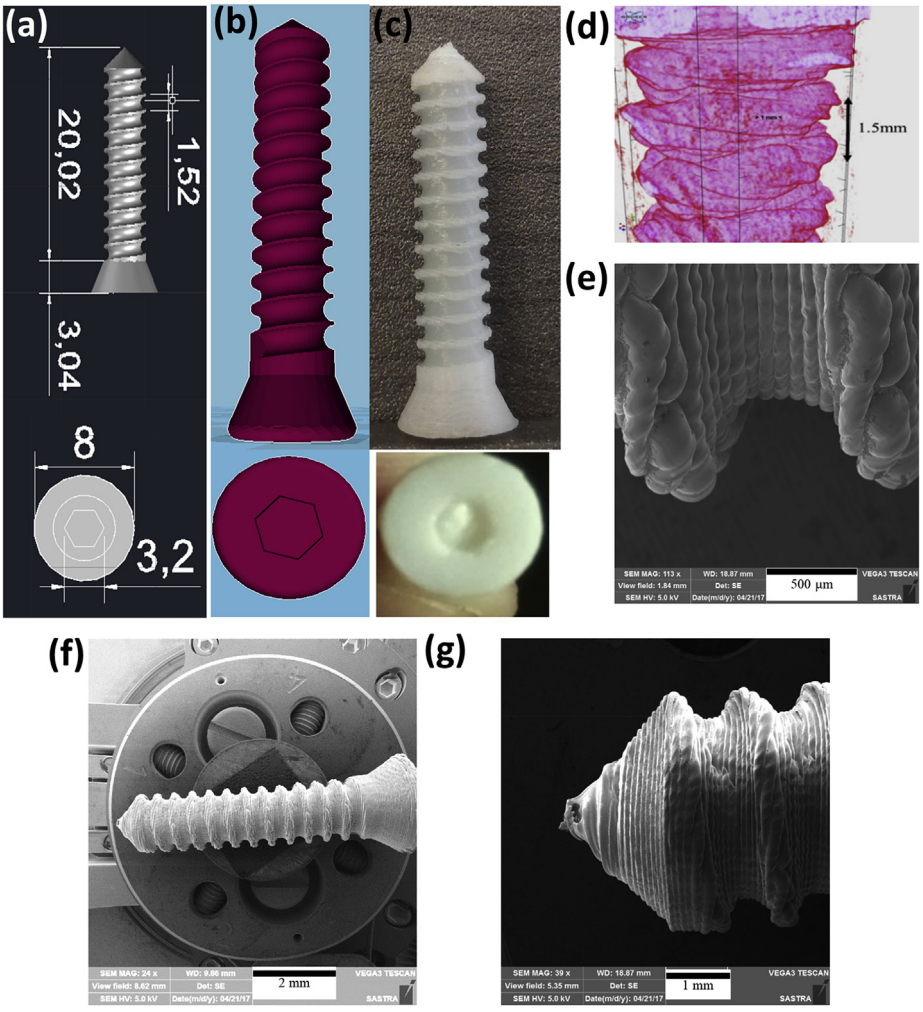

Fig. 2. (a) AUTOCAD designed screw in mm; (b) STL file shows the 3D printable screw model; (c) 3D Printed cortical screw; (d & e) pitch length of printed screw measured using micro CT and SEM (f & g) uniform layers were observed forming rough surface from head till tapered end.

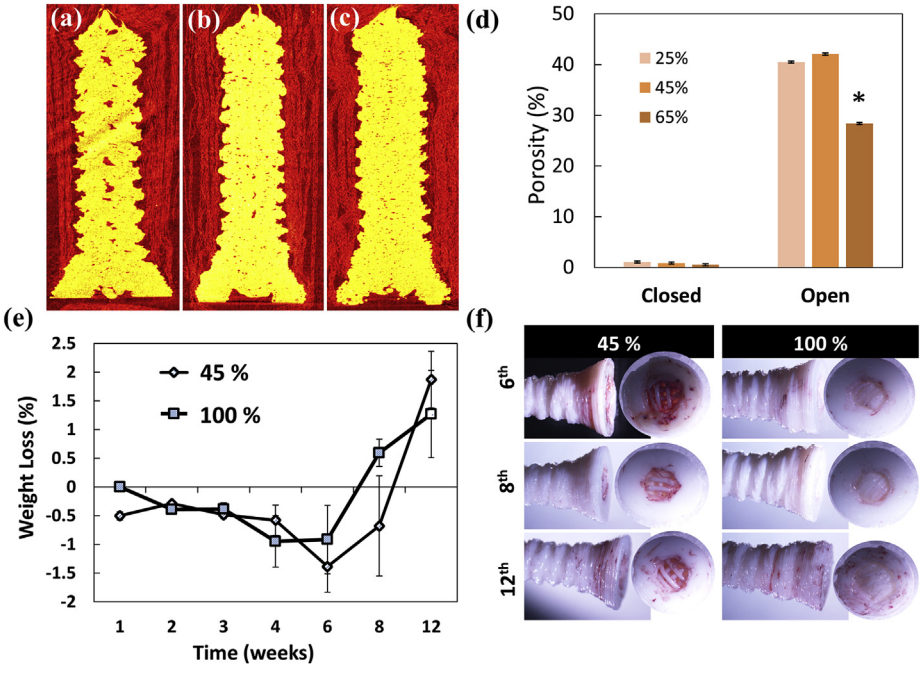

Fig. 3. Micro CT sections of porous screws with FD (a) 25%, (b) 45%, & (c) 65%; (d) pore distribution in the porous screws analyses using micro CT (*p < 0.05); (e) Biodegradation profile of porous versus solid screws over 12 weeks incubation in simulated body fluid; (f) alizarin red stained screws substantiate better mineralization in 45% screws.

Table 3
Compressive and torsional analysis of 45% and 100% screws.

Screws	Compressive Strength (MPa)	Maximum Load (N)	Elastic Modulus (MPa)	Peak Torque (Nm)	Break angle (°)
45%	24.58 ± 1.36	482.79 ± 26.62	412.77 ± 27.94	0.384 ± 0.038	490.50 ± 79.67
100%	26.13 ± 0.56	513.04 ± 11.96	548.19 ± 58.92	0.530 ± 0.017	401.54 ± 40.49

any distortion by optimizing printing parameters such as print speed, travel speed and layer height. Print speed controls the velocity of extruder movement during filament extrusion where slower rate achieved better shape and resolution of prototype. Minimizing the travel speed reduced the extruder motion induced vibrations resulted in stable undistorted screw structures (Fig. 1). Layer height increased the distance between Z-axis layers, which would avoid the layer coalescence. Fill density had been varied to obtain desirable pore dimensions, open porosity and layer thickness in the screw stem.

Screws were designed using AUTOCAD similar to commercially available 4.5 mm cortical screws and 3D printed using biodegradable and biocompatible PLA filament. According to the standards, three main elements viz., the number of threads per inch, pitch and thread diameter, were found to exactly match with standard titanium screws, thus proving the method to be highly efficient and precise for the fabrication of porous biodegradable screws. Characterization of porous and solid screws using SEM and μCT showed higher interconnected porosity for 45% FD screws. This matched with optimum porosity of 30–40% for bone scaffolds that have shown better bone regeneration and bone regrowth [36]. Hence, further studies were carried out with 45% FD screws in comparison to 100% FD screws (solid screws). *In vitro* biodegradation in SBF showed increasing weights over 12 weeks duration, which can be correlated to the deposition of salts in the screws. By-products of PLA support apatite formation by the precipitation of calcium phosphate crystals present in SBF which promotes mineralization of bone scaffolds, thus resulting in apatite formation and bone regeneration [37]. Porous interconnectivity did not alter the compressive strength of the screws. Larger gap between the stiffness of metallic screws and native tissue shares the load disproportionately resulting in stress induced atrophy. Lower elastic modulus of printed screws with 482.79 ± 26.62 MPa (porous) and 513.04 ± 11.96 MPa (solid) in comparison with titanium (110 GPa) and stainless steel (210 GPa) would protect the host tissue from atrophy [38]. Torsional assessment of screws directly correlates with the anchorage ability of screws to bone. Further polymeric screws were reported to reorganize polymeric chains to counteract the applied torque during fixation, which may causes physical relaxation and enhance host tissue integration in contrary to the titanium screws [39]. Biocompatible and cellular proliferation efficacy of screws was evaluated using osteoblast-like cells and BMSCs. Cell–screw interactions were evident in scanning electron and fluorescence micrographs. Significantly higher alkaline phosphatase activity of cultured MG63 cell lines on porous screws confirms the potential of these screws on mineralization of neotissue. Further, alizarin red staining assay demonstrates the osteogenic differentiation and mineralization of BMSCs proliferating on porous screws in comparison with solid screws. It may be attributed that the porous interconnections may ease the diffusion of desirable nutrients for osteogenic differentiation and intensified calcium deposits by extending nucleation sites [40]. Evaluation of local tissue reactions for both porous and solid screws based on the ISO 10993-6-2007 confirmed non-irritant characteristics of screws by *in vivo* scoring. Bands of capillaries with fibroblastic support structures from first week of implantation demonstrated the angiogenic potential of porous screws than solid screws. Since the extent of neovascularisation is strongly related to osteogenesis, bone remodeling and fracture repair, biodegradable porous screws would be promising substitute for rapid healing of fractured tissue and vascularized bone ingrowth [21].

6. Conclusion

Fused deposition modeling based 3D printing technology has been employed to fabricate biodegradable cortical screws with porous interconnections which cannot be achieved using conventional screw moulding technique. Developed porous biodegradable screws showed

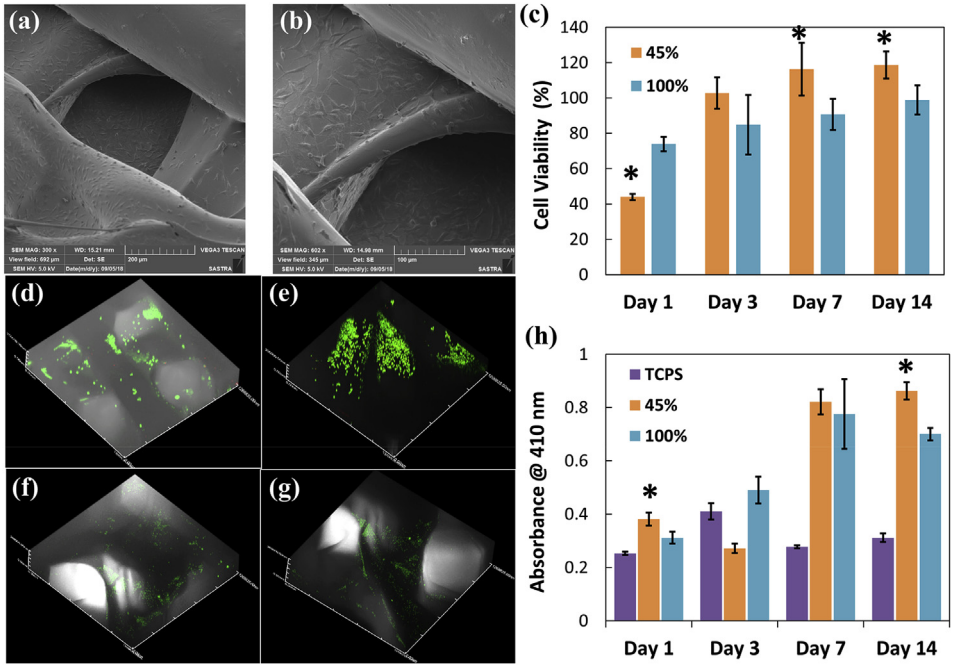

Fig. 4. (a) & (b) Scanning electron micrographs of fully extended MG63 cells on porous screws after 3 days of culture (305X and 602X; scale bar 100 μm); (c) cytocompatibility of 45% and 100% screws with MG63 cells for 14 days (*p < 0.05); Z-stacked images of live/dead stained MG63 cells on porous screws on (d) day 1, (e) day 3, (f) day 7, (g) day 14; (h) alkaline phosphatase activity of MG63 increased for 45% than 100% screws, *p < 0.05.

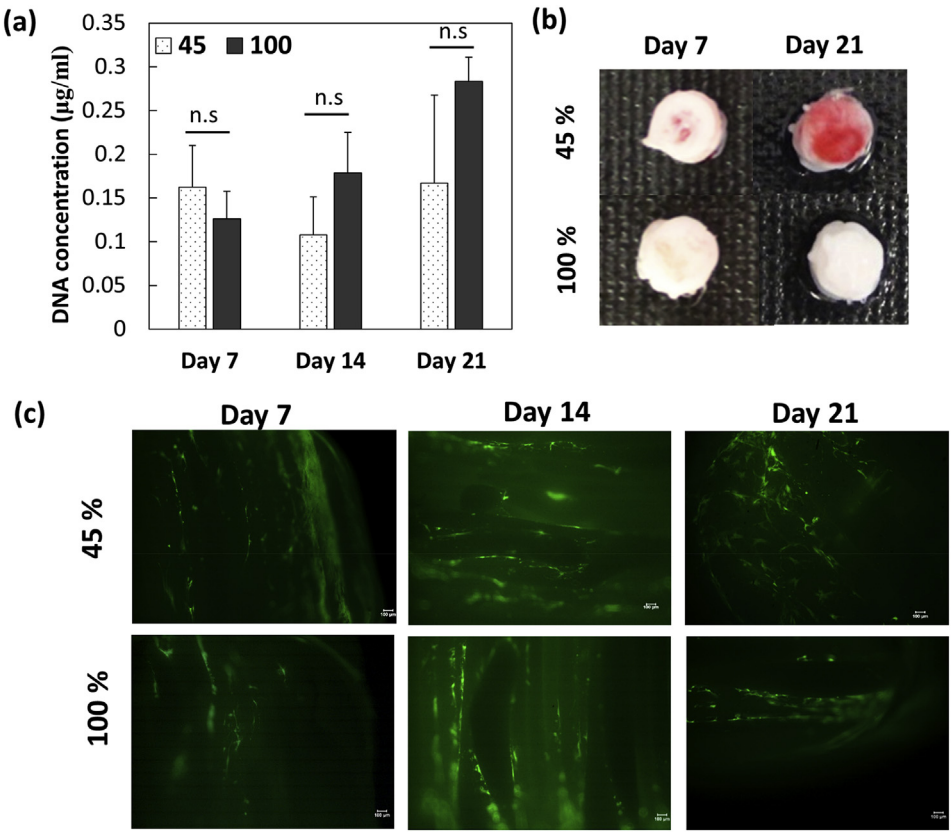

Fig. 5. (a) Quantification of DNA in BMSCs showed increasing cell number in 45% and 100% screws; (b) alizarin red staining was predominantly higher in porous screws; (c) calcein stained live cells were located on the screw surface on 100% screws whereas cells were observed even in between pores in 45% screws (scale bar 100 µm).

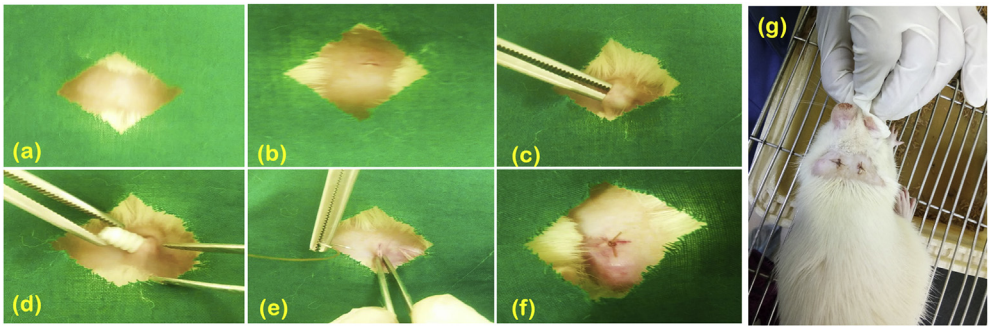

Fig. 6. Subcutaneous implantation of screws in Wistar Rats was carried out by exposing the (a) shaved neck region; (b) incision was made using surgical blade further; (c) subcutaneous pouch was created; (d) the screws were implanted subcutaneously; (e) Pouch was closure using suture; (f) after implantation and (g) dorsal region of rat after surgery.

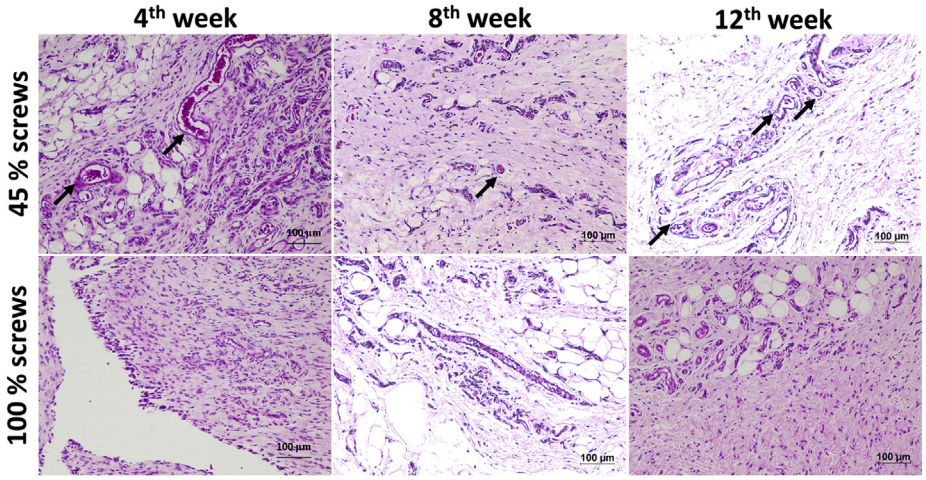

Fig. 7. Histopathological section of subcutaneous tissue surrounding the implant after 4, 8 and 12 weeks of implantation showed better neovascularisation (black arrows) in H&E staining in porous screws (10X magnification, 100 µm scale bar).

interconnected pores similar to native bone tissue (~300 μm) without compromising the mechanical strength thereby preventing the stress-shielding effect. *In vitro* biodegradation of porous screws showed enhanced mineralization over four weeks which can be correlated with the presence of pores that would act as nucleation sites for salt deposition. BMSCs cultured on the screws confirmed differentiation towards osteoblast lineage and similarly osteoblast-like cells cultured over 21 days showed mineralization with largely infiltrated cells in porous screws. Biocompatibility evaluation by subcutaneous implantation in rats revealed that porous screws increased neovascularisation and showed low immunogenicity around the implant site when compared to the non-porous screws. Future studies are aimed at evaluating osteointegration and healing rate of porous screws implanted in critical defect animal model.

CRediT authorship contribution statement

Ramya Dhandapani: Formal analysis, Investigation, Writing - original draft. **Priya Dharshini Krishnan:** Formal analysis, Investigation. **Allen Zennifer:** Investigation. **Vishal Kannan:** Investigation. **Amrutha Manigandan:** Investigation. **Michael R. Arul:** Formal analysis, Investigation. **Devina Jaiswal:** Formal analysis, Investigation. **Anuradha Subramanian:** Methodology, Validation, Writing - review & editing. **Sangamesh Gurappa Kumbar:** Conceptualization, Funding acquisition, Writing - review & editing. **Swaminathan Sethuraman:** Conceptualization, Funding acquisition, Writing - review & editing.

Declaration of competing interest

Authors have no conflict of interest.

Acknowledgements

Authors would like to acknowledge funding from the Indo-US Science and Technology Forum-JC-26-2014. Dr. Kumbar acknowledges funding from the National Institute of Biomedical Imaging and Bioengineering of the National Institutes of Health-R01EB020640 and the Connecticut Regenerative Medicine Research Fund (15-RMBUCHC-08). First Author is thankful to the Council of Scientific and Industrial Research for senior research fellowship (09/1095(0022)/18-EMR-I), Government of India. Third Author would like to thank Innovation in Science Pursuit for Inspired Research (INSPIRE), DST, India for Junior Research Fellowship (IF150843).

References

[1] P. Pisani, M.D. Renna, F. Conversano, E. Casciaro, M. Di Paola, E. Quarta, M. Muratore, S. Casciaro, Major osteoporotic fragility fractures: risk factor updates and societal impact, World J. Orthoped. 7 (2016) 171–181, https://doi.org/10.5312/wjo.v7.i3.171.

[2] Y. Chen, M. Sebag, T.I. Powell, S.N. Morin, Atypical femur fracture in a woman with osteogenesis imperfecta and multiple myeloma, J. Musculoskelet. Neuronal Interact. 18 (2018) 375.

[3] N.K. Sahoo, S.C. Anand, J.R. Bhardwaj, V.P. Sachdeva, B.L. Sapru, Bone response to stainless stell and titanium bone plates: an Experimental Study on Animals, Med. J. Armed Forces India 50 (1994) 10–14.

[4] T.A. Einhorn, L.C. Gerstenfeld, Fracture healing: mechanisms and interventions, Nat. Rev. Rheumatol. 11 (2015) 45.

[5] A.S. Moisala, T. Järvelä, A. Paakkala, T. Paakkala, P. Kannus, M. Järvinen, Comparison of the bioabsorbable and metal screw fixation after ACL reconstruction with a hamstring autograft in MRI and clinical outcome: a prospective randomized study, Knee Surg. Sports Traumatol. Arthrosc. 16 (2008) 1080–1086, https://doi.org/10.1007/s00167-008-0593-z.

[6] C. Marti, A.B. Imhoff, C. Bahrs, J. Romero, Metallic versus bioabsorbable interference screw for fixation of bone–patellar tendon–bone autograft in arthroscopic anterior cruciate ligament reconstructiont, Knee Surg. Sports Traumatol. Arthrosc. 5 (1997) 217–221, https://doi.org/10.1007/s001670050053.

[7] P.F. Stahel, N.A. Alfonso, C. Henderson, T. Baldini, Introducing the "Bone-Screw-Fastener" for improved screw fixation in orthopedic surgery: a revolutionary paradigm shift? Patient Saf. Surg. 11 (2017) 6.

[8] J. Wang, J. Xu, W. Fu, W. Cheng, K. Chan, P.S. Yung, L. Qin, Biodegradable magnesium screws accelerate fibrous tissue mineralization at the tendon-bone insertion in anterior cruciate ligament reconstruction model of rabbit, Sci. Rep. 7 (2017) 40369, https://doi.org/10.1038/srep40369.

[9] W.J. Chang, Y.H. Pan, J.J. Tzeng, T.L. Wu, T.H. Fong, S.W. Feng, H.M. Huang, Development and testing of X-ray imaging-enhanced poly-L-lactide bone screws, PLoS One 10 (2015) 1–12, https://doi.org/10.1371/journal.pone.0140354.

[10] S. Zhang, Q. Yang, W. Zhao, B. Qiao, H. Cui, J. Fan, H. Li, X. Tu, D. Jiang, In vitro and in vivo biocompatibility and osteogenesis of graphene-reinforced nanohydroxyapatite polyamide66 ternary biocomposite as orthopedic implant material, Int. J. Nanomed. 11 (2016) 3179–3189, https://doi.org/10.2147/IJN.S105794.

[11] G.S. Perrone, G.G. Leisk, T.J. Lo, J.E. Moreau, D.S. Haas, B.J. Papenburg, E.B. Golden, B.P. Partlow, S.E. Fox, A.M.S. Ibrahim, S.J. Lin, D.L. Kaplan, The use of silk-based devices for fracture fixation, Nat. Commun. 5 (2014) 1–9, https://doi.org/10.1038/ncomms4385.

[12] S. Cox, D.P. Mukherjee, A.L. Ogden, R.H. Mayuex, K.K. Sadasivan, J.A. Albright, W.S. Pietrzak, Distal tibiofibular syndesmosis fixation: a cadaveric, simulated fracture stabilization study comparing bioabsorbable and metallic single screw fixation, J. Foot Ankle Surg. 44 (2005) 144–151, https://doi.org/10.1053/j.jfas.2005.01.010.

[13] D.M. Ramos, R. Dhandapani, A. Subramanian, S. Sethuraman, S.G. Kumbar, Clinical complications of biodegradable screws for ligament injuries, Mater. Sci. Eng. C 109 (2020) 110423, https://doi.org/10.1016/j.msec.2019.110423.

[14] S. Huang, P. He, D. Xu, J. Li, X. Peng, Y. Tang, Acidic stress induces apoptosis and inhibits angiogenesis in human bone marrow-derived endothelial progenitor cells, Oncol. Lett. 14 (2017) 5695–5702.

[15] A. Chaya, S. Yoshizawa, K. Verdelis, N. Myers, B.J. Costello, D.-T. Chou, S. Pal, S. Maiti, P.N. Kumta, C. Sfeir, In vivo study of magnesium plate and screw degradation and bone fracture healing, Acta Biomater. 18 (2015) 262–269, https://doi.org/10.1016/j.actbio.2015.02.010.

[16] S.J. Hollister, Porous scaffold design for tissue engineering, Nat. Mater. 5 (2006), https://doi.org/10.1038/nmat1683 590–590.

[17] D.W. Hutmacher, Scaffold design and fabrication technologies for engineering tissues — state of the art and future perspectives, J. Biomater. Sci. Polym. Ed. 12 (2001) 107–124, https://doi.org/10.1163/156856201744489.

[18] A. Strobel, Michael and Weiler, Andreas and Timmermans, Biodegradable Interference Screw and Tool for Attaching a Transplant to a Bone, (2007).

[19] A. Weiler, H.J. Windhagen, M.J. Raschke, A. Laumeyer, R.F.G. Hoffmann, Biodegradable interference screw fixation exhibits pull-out force and stiffness similar to titanium screws, Am. J. Sports Med. 26 (1998) 119–128.

[20] J. Bergsma, Late degradation tissue response to poly(L-lactide) bone plates and screws, Biomaterials 16 (1995) 25–31, https://doi.org/10.1016/0142-9612(95)91092-D.

[21] V. Karageorgiou, D. Kaplan, Porosity of 3D biomaterial scaffolds and osteogenesis, Biomaterials 26 (2005) 5474–5491, https://doi.org/10.1016/j.biomaterials.2005.02.002.

[22] J.A. Slotwinski, E.J. Garboczi, K.M. Hebenstreit, Porosity measurements and analysis for metal additive manufacturing process control, J. Res. Natl. Inst. Stand. Technol. 119 (2014) 494–528, https://doi.org/10.6028/jres.119.019.

[23] A.L. Jardini, M.A. Larosa, R. Maciel Filho, C.A. de Carvalho Zavaglia, L.F. Bernardes, C.S. Lambert, D.R. Calderoni, P. Kharmandayan, Cranial reconstruction: 3D biomodel and custom-built implant created using additive manufacturing, J. Cranio-Maxillofacial Surg. 42 (2014) 1877–1884.

[24] B. Wysocki, P. Maj, R. Sitek, J. Buhagiar, Laser and electron beam additive manufacturing methods of fabricating titanium bone implants, Appl. Sci. 7 (2017) 1–20, https://doi.org/10.3390/app7070657.

[25] L.E. Murr, A metallographic review of 3D printing/additive manufacturing of metal and alloy products and components, Metallogr. Microstruct. Anal. 7 (2018) 103–132.

[26] C. Gao, C. Wang, H. Jin, Z. Wang, Z. Li, C. Shi, Y. Leng, F. Yang, H. Liu, J. Wang, Additive manufacturing technique-designed metallic porous implants for clinical application in orthopedics, RSC Adv. 8 (2018) 25210–25227.

[27] K. Tappa, U. Jammalamadaka, J.A. Weisman, D.H. Ballard, D.D. Wolford, C. Pascual-Garrido, L.M. Wolford, P.K. Woodard, D.K. Mills, 3D printing custom bioactive and absorbable surgical screws, pins, and bone plates for localized drug delivery, J. Funct. Biomater. 10 (2019) 17.

[28] C.L. Ventola, Medical applications for 3D printing: current and projected uses, P T 39 (2014) 704–711, https://doi.org/10.1016/j.infsof.2008.09.005.

[29] B. Berman, 3-D printing: the new industrial revolution, Bus. Horiz. 55 (2012) 155–162, https://doi.org/10.1016/j.bushor.2011.11.003.

[30] S. Jalota, S.B. Bhaduri, A.C. Tas, In vitro testing of calcium phosphate (HA, TCP, and biphasic HA-TCP) whiskers, J. Biomed. Mater. Res. Part A an off, J. Soc. Biomater. Japanese Soc. Biomater. Aust. Soc. Biomater. Korean Soc. Biomater. 78 (2006) 481–490.

[31] K. Kapat, P.K. Srivas, A.P. Rameshbabu, P.P. Maity, S. Jana, J. Dutta, P. Majumdar, D. Chakrabarti, S. Dhara, Influence of porosity and pore-size distribution in Ti6Al4V foam on physicomechanical properties, osteogenesis, and quantitative validation of bone ingrowth by micro-computed tomography, ACS Appl. Mater. Interfaces 9 (2017) 39235–39248.

[32] J.-H. Kühne, R. Bartl, B. Frisch, C. Hammer, V. Jansson, M. Zimmer, Bone formation in coralline hydroxyapatite: effects of pore size studied in rabbits, Acta Orthop. Scand. 65 (1994) 246–252.

[33] A.R. Amini, D.J. Adams, C.T. Laurencin, S.P. Nukavarapu, Optimally porous and biomechanically compatible scaffolds for large-area bone regeneration, Tissue Eng. Part A. 18 (2012) 1376–1388, https://doi.org/10.1089/ten.TEA.2011.0076.

[34] F.W. Sunderman Jr., S.M. Hopfer, T. Swift, W.N. Rezuke, L. Ziebka, P. Highman, B. Edwards, M. Folcik, H.R. Gossling, Cobalt, chromium, and nickel concentrations

in body fluids of patients with porous-coated knee or hip prostheses, J. Orthop. Res. 7 (1989) 307–315.
[35] H. Cui, S. Miao, T. Esworthy, X. Zhou, S.-J. Lee, C. Liu, Z.-X. Yu, J.P. Fisher, M. Mohiuddin, L.G. Zhang, 3D bioprinting for cardiovascular regeneration and pharmacology, Adv. Drug Deliv. Rev. 132 (2018) 252–269, https://doi.org/10.1016/j.addr.2018.07.014.
[36] J. Will, R. Melcher, C. Treul, N. Travitzky, U. Kneser, E. Polykandriotis, R. Horch, P. Greil, Porous ceramic bone scaffolds for vascularized bone tissue regeneration, J. Mater. Sci. Mater. Med. 19 (2008) 2781–2790, https://doi.org/10.1007/s10856-007-3346-5.
[37] J.J. Kim, S.H. Bang, A. El-Fiqi, H.W. Kim, Fabrication of nanofibrous macroporous scaffolds of poly(lactic acid) incorporating bioactive glass nanoparticles by camphene-assisted phase separation, Mater. Chem. Phys. 143 (2014) 1092–1101, https://doi.org/10.1016/j.matchemphys.2013.11.009.
[38] C. Kaeding, J. Farr, T. Kavanaugh, A. Pedroza, A prospective randomized comparison of bioabsorbable and titanium anterior cruciate ligament interference screws, Arthrosc. J. Arthrosc. Relat. Surg. 21 (2005) 147–151, https://doi.org/10.1016/j.arthro.2004.09.012.
[39] G.J. Buijs, E.B. Van Der Houwen, Torsion Strength of Biodegradable and Titanium Screws : A Comparison, (2007), pp. 2142–2147, https://doi.org/10.1016/j.joms.2007.08.002.
[40] C. Shuai, H. Sun, P. Wu, C. Gao, Y. Yang, W. Guo, D. Yang, F. Xu, P. Feng, S. Peng, Biosilicate scaffolds for bone regeneration: influence of introducing SrO, RSC Adv. 7 (2017) 21749–21757.